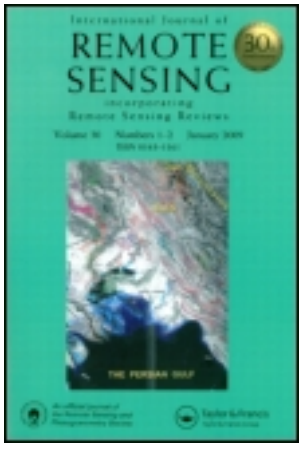

International Journal of Remote Sensing
Publication details, including instructions for authors and subscription information:
http://www.tandfonline.com/loi/tres20

Lidar-based change detection and change-type determination in urban areas

Tee-Ann Teo [a] & Tian-Yuan Shih [a]
[a] Department of Civil Engineering , National Chiao Tung University , Hsinchu , Taiwan
Published online: 02 Oct 2012.

To cite this article: Tee-Ann Teo & Tian-Yuan Shih (2013) Lidar-based change detection and change-type determination in urban areas, International Journal of Remote Sensing, 34:3, 968-981, DOI: 10.1080/01431161.2012.714504

To link to this article: http://dx.doi.org/10.1080/01431161.2012.714504

International Journal of Remote Sensing
Vol. 34, No. 3, 10 February 2013, 968–981

Taylor & Francis
Taylor & Francis Group

Lidar-based change detection and change-type determination in urban areas

Tee-Ann Teo* and Tian-Yuan Shih

Department of Civil Engineering, National Chiao Tung University, Hsinchu, Taiwan

(*Received 27 February 2011; accepted 6 September 2011*)

Change detection of objects, such as buildings, is essential for map updating. Traditionally, detection is usually performed through spectral analysis of multi-temporal images. This article proposes a method that employs multi-temporal interpolated lidar data. The objective of this study is to perform change detection and change-type determination via geometric analysis. A shape difference map is generated between the digital surface models in two different time periods. The areas with small shape differences are treated as non-changed areas and are excluded from the segmentation. The object's properties are then applied to determine the change types. Experimental results demonstrate that the proposed scheme achieves accuracy as high as 80%. Most of the errors from this study occurred in small or vegetation areas.

1. Introduction

Change detection is a vital task in geoinformatics. A type of change of particular interest to those involved in sustainable urban development is that relating to buildings in urban areas. Such changes may be due to human activities, such as construction, or caused by natural disasters (Vu and Ban 2010), such as earthquakes. The results of building change detection are useful in many areas including urban management, disaster management, and updating map and geographical information system (GIS) databases (Knudsen and Olsen 2003; Vosselman, Gorte, and Sithole 2004). With ever-increasing amounts of data being made available, improving the degree of automation and the quality of change detection is essential in a dynamic urban environment (Matikainen, Hyyppä, and Hyyppä 2004; Rottensteiner 2008; Caelen 2010).

Remote sensing is a useful technology to acquire timely land-cover information from a large area. Multi-temporal image and surface data sets with different spatial scales are commonly used in change detection (Steinnocher and Kressler 2006; Champion et al. 2008), with spectral information from the image data particularly useful in the identification of regions of change (Stamm and Briggs 1999; Im, Jensen, and Tullis 2008; Li, Xu, and Guo 2010). However, image quality is critical to the accuracy of identifying such regions, especially when shadows and occlusions affect the results. Moreover, change detection from spectral information usually provides only 2D information about changes. Three-dimensional surface data can be obtained by matching stereo images or from airborne light detection and ranging (lidar). Multi-temporal surface data can be analysed to determine

*Corresponding author. Email: tateo@mail.nctu.edu.tw

ISSN 0143-1161 print/ISSN 1366-5901 online

http://dx.doi.org/10.1080/01431161.2012.714504
http://www.tandfonline.com

shape differences for change detection (Vögtle and Steinle 2004). Such surface information may shed light on changes in 3D volumes rather than mere 2D regions.

Change detection from images is pixel-based. In multi-temporal images, corresponding pixels that exhibit large radiometric differences can be distinguished easily, for example, changes between vegetation and non-vegetation. It is one thing to identify that change has occurred, but another to identify the type of change. Pixel variation is not adequately informative to differentiate types of change in areas with similar spectral values, such as when buildings and roads have similar grey values. One possible solution is to group pixels into regions and study the region major axis, texture, and other additional information from the grouped pixels (Walter 2004, 2005).

The strategies for change detection can be classified into two categories. In the first category, changes are directly detected by comparing the attributes of data between two periods (Murakami, Nakagawa, and Hasegawa 1999). The attributes could involve spectral or height information. However, this method can lead to ambiguities because of the effect of shadows and relief displacement in the image space. The second strategy is to perform classification and then compare class similarities between the two periods (Bouziani, Goïta, and He 2010). The advantage of this method is that prior knowledge about land cover can be utilized when comparing corresponding regions from two periods.

Numerous studies have reported the use of surface data for change detection. Murakami, Nakagawa, and Hasegawa (1999) employed multi-temporal airborne lidar data to detect changes in buildings by direct surface comparison. They also used shrinking and expansion filters to remove small areas caused by horizontal errors in the lidar data. Data fusion may be used to combine information from different sensors. Imagery and its complementary counterpart, elevation, can be integrated into the change detection process. Vu, Matsuoka, and Yamazaki (2004) used airborne lidar and a natural colour aerial image to detect and classify buildings based on elevation and intensity information. Intensity information from lidar data is combined with red bands from aerial photographs to exclude areas of vegetation. Jung (2004) proposed a two-state change detection method, comparing both surface data and grey values. The surface data are generated by image matching and used to eliminate those areas without change. The grey values from multiple images of candidate regions are then compared to determine the changed areas.

Several studies have adopted existing maps and remotely sensed data. Knudsen and Olsen (2003) integrated vector maps and spectral data in unsupervised spectral classification. The classified pixels were subsequently defined as ‘no change’, ‘potential change’, and ‘evident change’ using predefined rules. Matikainen, Hyyppä, and Hyyppä (2004) detected changes in buildings using a method combining lidar and image data. They compared the detected buildings with building locations from existing maps and applied the change information to update the maps. Bouziani, Goïta, and He (2010) performed change detection in an urban area from extremely high-resolution satellite images and existing maps. Map-guided change detection and prior knowledge from maps were utilized to enhance the capability of image interpretation. The detection rate reached 90%.

Although several researchers have used image and surface data for change detection in urban areas, relatively few studies have considered identifying the type of change. The purpose of this study is to address this issue. This study applies multi-temporal interpolated lidar data to object-based change detection. The objects involved regions with large height differences. The change-type determination is based on some predefined rules of object properties. Increasing the knowledge of change behaviour in urban areas is, therefore, possible.

2. Methodology

The proposed method comprises four major parts. In the first part, preprocessing (interpolation and spatial coregistration of multi-temporal lidar data) is conducted. The second part involves mapping the segmentation of change based on height differences. In the third part, buildings and vegetation objects are classified according to surface roughness. The final step involves determining the type of change for each object. Figure 1 shows the work flow of the proposed method. Details of each step are provided below.

2.1. Data preprocessing

The first step of change detection is data coregistration. Data coregistration may provide uniform geometry between different data sets. Problems with non-uniform geometry between different data sets may cause faulty change detection. Therefore, aligning the two lidar data sets into a unified system is critical. The procedures of data coregistration include the selection of registration entities and the calculation of transformation parameters. The registration entities such as conjugate surface (Gruen and Akca 2005), conjugate line (Jaw and Chuang 2008), and conjugate point can be selected automatically or manually. As the changed areas may affect the automatic process, numerous registration points were manually selected using lidar intensity data. An area with height discontinuities is not suitable for selecting a registration point; hence, we mainly measure the registration points that are on the road surface (e.g. pedestrian crossing). In the calculation of transformation parameters, 3D similarity transformation consisting of three translations, three rotations, and one scale factor is usually selected to compensate the error between multiple lidar strips. The situation of this study is different from lidar strip adjustment, because the test data in this study are the product that have been converted to world coordinates using ground control points. In order to correct the bias between the two rigid bodies and to avoid over-parameterization, only three translations are calculated from registration points using least squares adjustment. Finally, the three translations are used to adjust the 3D points acquired at different times.

Lidar point clouds include 3D coordinates for ground points and surface points. These two sets of data may be used to generate digital terrain models (DTMs) and digital surface models (DSMs) in a grid format (Behan 2000; Briese, Pfeifer, and Dorninger 2002). The ground points were processed with automated filtering (Axelsson 2000) followed

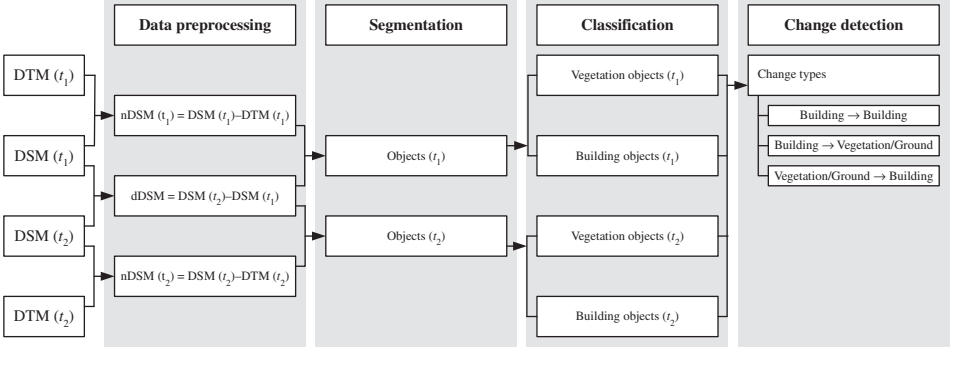

Figure 1. Workflow of the proposed method.

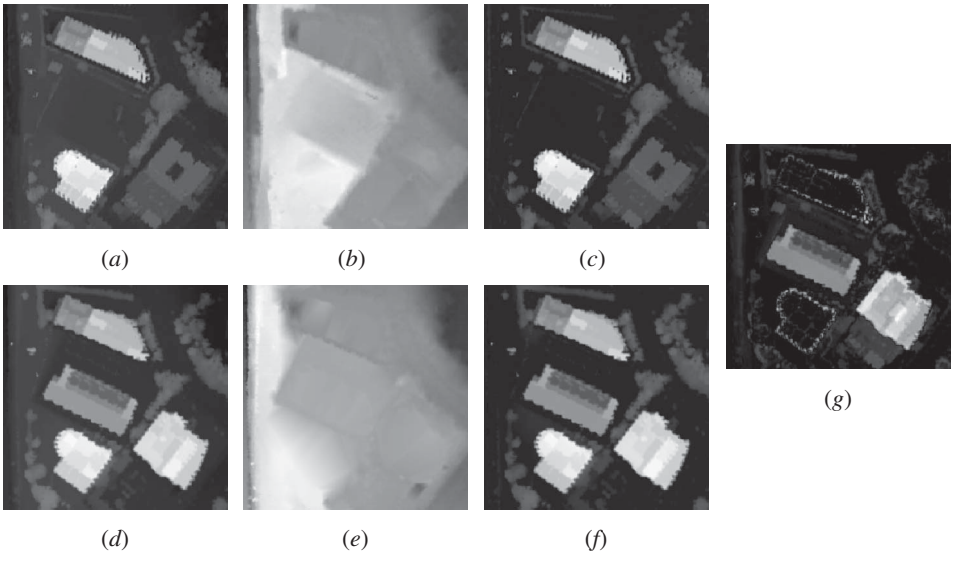

Figure 2. Illustration of data preprocessing: (*a*) DSM at time 1; (*b*) DTM at time 1; (*c*) nDSM at time 1; (*d*) DSM at time 2; (*e*) DTM at time 2; (*f*) nDSM at time 2; (*g*) dDSM between time 1 and time 2.

by a manual editing procedure (TerraSolid 2004). A more detailed discussion of ground point selection can be found in Sithole and Vosselman (2004). The DTM was subtracted from the DSM to obtain the normalized DSM (nDSM). The nDSM was calculated using Equation (1). Two nDSMs with different periods were generated to describe the above-ground height information. An elevation threshold was established to separate the object above the ground from the nDSM. The above-ground surfaces include buildings and vegetation that are higher than the elevation threshold. Figures 2(*a*)–(*c*) show examples of a DSM, DTM, and nDSM from the earlier period. Figures 2(*d*)–(*f*) show examples of a DSM, DTM, and nDSM from a later period.

After registration, the DSM of the later period was subtracted from that of the former period to obtain delta DSM (dDSM). The dDSM was obtained using Equation (2). The benefit of generating this height difference map is to locate the potential change area. Hence, the proposed method does not include the unchanged areas in change-type determination in order to avoid misclassification and improve the computation performance. This height difference map indicates areas with differences in 3D surfaces. Unfortunately, all types of changes are mixed in a single difference map. Hence, additional processing was required in this study to separate the change types. Figure 2(*g*) shows an example of a dDSM between two surface models. The bright areas indicate differences in height. The noisy boundaries are the result of the edge effect caused by interpolation errors.

$$\mathrm{nDSM}(t) = \mathrm{DSM}(t) - \mathrm{DTM}(t), \tag{1}$$

$$\mathrm{dDSM} = \mathrm{DSM}(t_2) - \mathrm{DSM}(t_1), \tag{2}$$

where DSM(t) is the DSM at time t, DTM(t) is the DTM at time t, nDSM(t) is the nDSM at time t, dDSM is the dDSM between two periods, and t is time.

2.2. Segmentation

The objective of segmentation is to determine changed regions between two periods. The idea of segmentation is to extract the above-ground object from the nDSM and the height difference object from the dDSM. This study assumed that changed regions are mainly caused by changes in the above-ground objects. The terrain change was relatively small and could be ignored.

The height variation between two periods was included in the dDSM. However, this data set often contains commission errors, which arise due to interpolation errors in the regions near the step edge. To overcome this problem, a height threshold was applied to remove those areas with only a small height variation. A morphological filter, which includes erosion and dilation, was then applied to minimize these effects. This morphological filter could eliminate small regions and connect objects with small gaps. After this, a region growing technique was applied to the data. The criterion of region growing is the connectivity of pixels. All the connected pixels were grouped into regions. The area of each region could be determined after the region growing process was completed. Regions that cover small areas tend to be classified as commission errors and eliminated by an area threshold. The procedure for region generation used for the dDSM was also applied in this study to the nDSMs from the two different periods. Figures 3(*a*)–(*f*) show a comparison of the data with and without filtering.

The regions in the nDSM represent the above-ground objects without change information. To reduce computation time, the regions in the nDSMs were not compared directly. Only above-ground objects with shape differences were selected to exclude the unchanged regions. Candidate changed regions were extracted from the nDSM and dDSM. In other words, the detected above-ground objects in the nDSM were projected onto the dDSM to extract change regions between two periods. These changed regions were the above-ground objects with large shape differences. The intersection of nDSM and dDSM was used to detect and locate the candidate changed regions. The changed regions were extracted using Equation (3). Figures 3(*g*)–(*h*) illustrate the results of segmentation. Figure 3(*g*) is generated from Figures 3(*b*) and (*d*). If the above-ground objects in Figure 3(*b*) have large height differences in Figure 3(*d*), then the above-ground objects are considered as changed regions, as shown in Figure 3(*g*). Figure 3(*h*) is generated from Figures 3(*d*) and (*f*) in the same scheme.

$$R(t) = \mathrm{nDSM}(t) \cap \mathrm{dDSM}, \tag{3}$$

where nDSM(t) is the nDSM at time t, dDSM is the dDSM between two periods, $R(t)$ is the changed region at time t, and t is time.

2.3. Classification

Each separated region after segmentation is a candidate object for classification. The geometric attributes, such as area, perimeter, and major axis, can be directly calculated from the regions. However, the regions do not have semantic attributes (such as building or vegetation), which are essential for change-type determination. Because the surface data provide only shape information, without spectral information, this study classified the surface data using surface roughness rather than a spectral index. In most cases, the surfaces of building rooftops are smoother than the surface of vegetation. Surface roughness is thus a suitable criterion for distinguishing between vegetation and building regions.

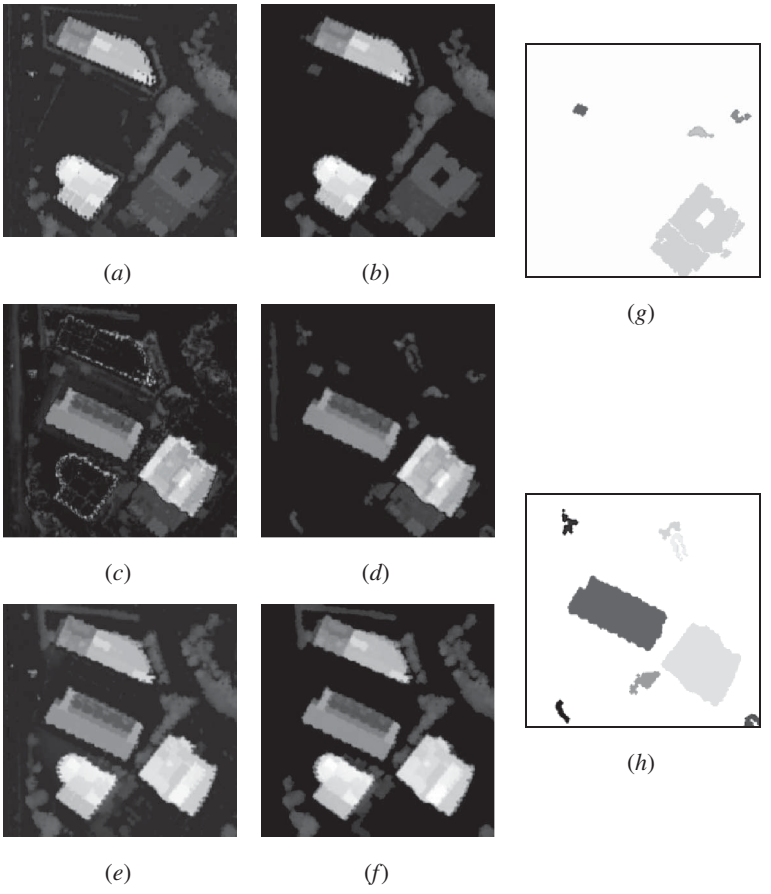

Figure 3. Illustration of data filtering and segmentation: (*a*) nDSM(t_1) before filtering; (*b*) nDSM(t_1) after filtering; (*c*) height difference before filtering; (*d*) dDSM between two periods; (*e*) nDSM(t_2) before filtering; (*f*) nDSM(t_2) after filtering; (*g*) segmentation results in t_1; (*h*) segmentation results in t_2.

The usefulness of roughness information for vegetation and building classification has been demonstrated in several studies (Mass 1999). Several methods determine the roughness of lidar data, such as the deviation of plane fitting and the echo width of a full-waveform laser pulase (Hollaus and Höfle 2010). The plane-fitting method calculates the deviation of points to best fit plane distance. A higher deviation of point-to-plane distance presents a higher roughness. This study uses raster data; therefore, the surface roughness was calculated by image-processing algorithms for gradient magnitude of the range image. This surface gradient contains the information about height discontinuities over a certain distance. The gradient of each pixel was calculated from the connected pixels in eight directions. To compare the roughness from plane fitting and surface gradient, the point-to-plane distance of plane fitting is perpendicular to the best-fit plane, while the surface gradient measures the height discontinuities perpendicular to the datum. Although the plane-fitting method is more flexible to handle large slope areas (e.g. vertical wall), it needs more computation time for the iterative process. In order to accelerate the proposed method, we simply use the gradient magnitude to represent the surface roughness.

This study calculated the gradient magnitude within a region, serving as the roughness criterion. Surface roughness is used to classify regions into vegetation and non-vegetation

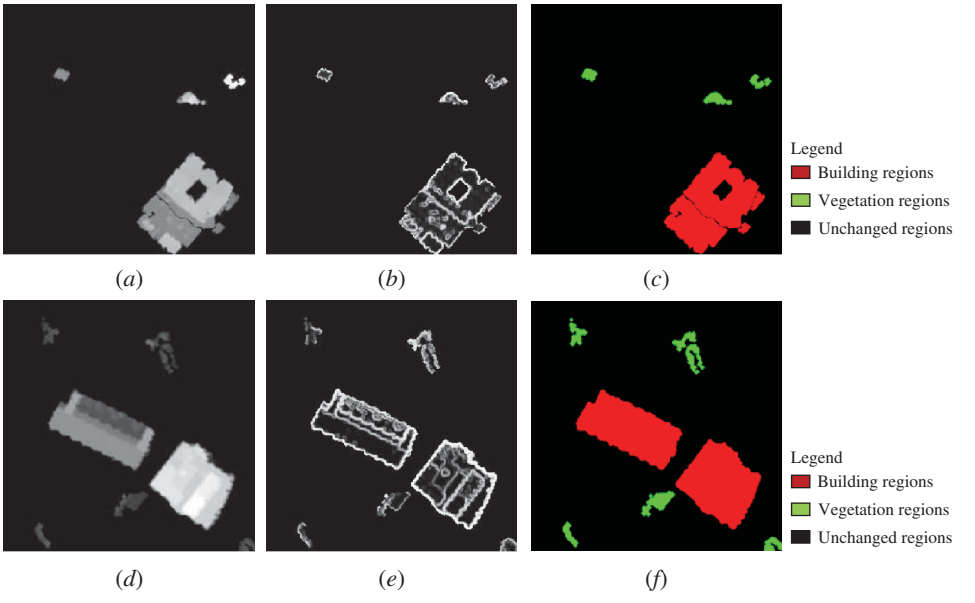

Figure 4. Example of classification: (*a*) nDSM(t_1) after segmentation; (*b*) roughness of nDSM(t_1); (*c*) classified results of nDSM(t_1); (*d*) nDSM(t_2) after segmentation; (*e*) roughness of nDSM(t_2); (*f*) classified results of nDSM(t_2).

regions. Two criteria were used for classification. The first was a gradient threshold, which was used to determine the point with the largest gradient variance. The second was an area threshold, which was used to determine the percentage of large gradients in a region. If the percentage of large gradients in a region was larger than the area threshold, the region was classified as a region of vegetation. Figure 4 demonstrates the results of classification.

2.4. Change-type determination

The change detection in an urban area is usually classified as either 'changed' or 'unchanged'. In other words, the classification is not adequately specific for some applications. Hence, this study defined several change types based on the attributes of the regions. Table 1 shows the categories of change types: 'changed building', 'newly built', and 'demolished building'. The change type was determined by comparing the attributes of the regions including land cover, height, and area. The 'changed building' is a building that has a different roof shape in two periods. The 'newly built' includes 'newly built from existing building-to-building' and 'newly built from non-building-to-building'. The 'newly

Table 1. Categories of change types.

Categories	Former period	Later period	Change of height	Changed of area
Changed building	Building	Building	Yes	No
Newly built from existing building-to-building	Building	Building	Yes	Yes
Newly built from non-building-to-building	Vegetation/ground	Building	Yes	Yes
Demolished building	Building	Vegetation/ground	Yes	Yes

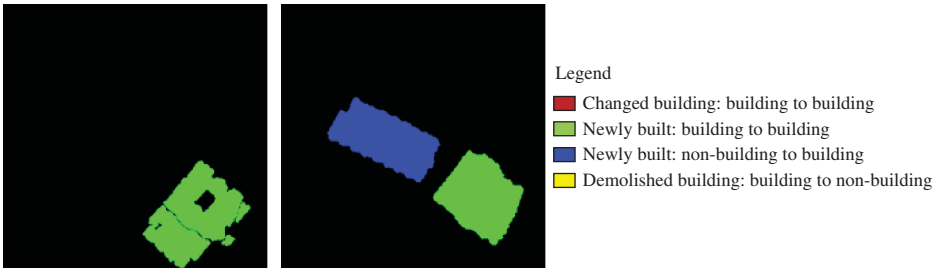

(*a*)

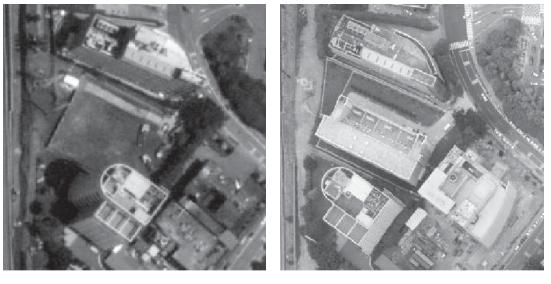

(*b*)

Figure 5. Example of change-type determination: (*a*) change type between two periods; (*b*) corresponding aerial images for the two periods.

built from existing building-to-building' represents that an old building in former period was destroyed and a new building appeared in latter period. The 'newly built from non-building-to-building' means a new building that appears distinct from a non-building to building. By contrast, the 'demolished building' is a building that changes from a building to a non-building.

Two major tasks are involved in change-type determination. First, the proposed method overlaps segmented regions from the two periods to build relationships between regions. An adjacency matrix is generated to link regions located in the same area but in two different periods. In the second part, all categories of change are defined by comparing the attributes of the regions. If the regions in the former time period do not have corresponding regions in the latter time period, these are defined as demolished buildings. Conversely, regions in the latter period that do not have corresponding regions in the former time period are marked as newly built. If the attribute in the two time periods is identified as a building, it could be either a changed building or a newly built one. Normally, the newly built building is shown by large changes of area. Thus, this study compared the area of the regions to separate changed and newly built buildings. Figure 5(*a*) illustrates an example of change type determination. The different colours indicate the different types of change. Figure 5(*b*) shows the corresponding aerial images for verification.

3. Results and discussion

3.1. Test data

The test site, located in Hsinchu City in northern Taiwan, has an area of 1083 m × 1963 m. The lidar point clouds were acquired using a Leica ALS40 and an ALS50 (Leica

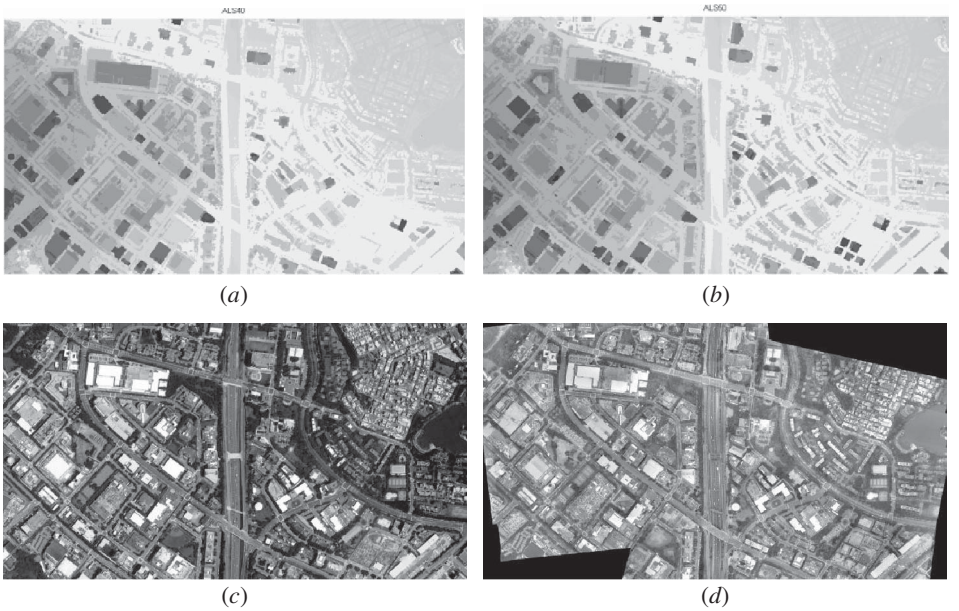

Figure 6. Test data: (*a*) lidar data for the year 2002; (*b*) lidar data for the year 2005; (*c*) reference orthoimage for the year 2002; (*d*) reference orthoimage for the year 2005.

Geosystems, Heerbrugg, Switzerland) in April 2002 and June 2005, respectively. The lidar data are shown in Figure 6. The average point densities are 1.85 and 1.93 points/m^2, respectively. As the point density in the overlapped area is higher than the average point density, and the across-track point spacing is better than 0.5 m, we consider oversampling the irregular points into a 0.5 m pixel. The surface points and ground points from the lidar data were rasterized to form the DSM and DTM (both with a pixel size of 0.5 m). The reference aerial images were acquired using a Leica RMK-TOP (Leica Geosystems, Heerbrugg, Switzerland) and Vexcel UltraCam-D camera (Microsoft Vexcel, Graz, Austria) in March 2002 and June 2005, respectively. The aerial images were rectified into orthoimages using the DSM with 0.25 m resolution. The orthoimages are shown in Figures 6(*c*)–(*d*). Notice that the orthoimages are for verification only. This study manually selected 10 registration points and 20 check points between lidars in different periods. The distribution of registration points covered the entire area. A simple translate function was applied to determine the transformation parameters. The mean and standard errors of check points were 0.05 and 0.08 m, respectively. After the alignment, the registration error became small and could be ignored.

3.2. Results

Several parameters must be considered in the proposed method. The numbers of the thresholds are provided based on prior knowledge obtained from existing data and training data. The parameters include the height of the above-ground objects, the window size of the morphological filter, the area for small objects, the flatness of objects with a small gradient, the roughness of the separation of vegetation and buildings, and the area difference between new and old buildings. All thresholds are summarized in Table 2.

Table 2. Change detection thresholds.

No	Items	Thresholds	Description
1	Height	3 m	To detect the above-ground objects in nDSM
2	Window size	2.5 m × 2.5 m	Window size for the erosion and dilation kernels
3	Small area	50 m^2	To remove small regions in the nDSM
4	Flatness	15°	To extract those pixels with small gradients from the region
5	Roughness	40%	If the percentage of large gradient pixels in a region is smaller than the threshold, then that region is treated as vegetation
6	Area difference	50 m^2	If, after calculating the difference between two periods, the area is larger than this threshold, then the region in the later period is treated as a new building

After the data preprocessing, segmentation was performed to group the pixels into regions. The segmentation results are shown in Figures 7(*a*) and (*b*). The regions with differences in shape were classified for further processing. Figures 7(*c*) and (*d*) show the results. All regions were classified as either buildings or vegetation. Finally, the type of change was obtained by examining the significant properties of these regions. The detected changed areas, together with the change types, are shown in Figures 7(*e*) and (*f*). Four examples are shown in Figure 8 to demonstrate various change types.

For accuracy assessment, the aerial images of the two periods were used as a reference. This verification provided quantitative results of the accuracy of the classification and change-type determination. The verification was performed by overlapping the regions and aerial orthoimages of the same area. The result was then manually verified. Finally, the accuracy of each change type was obtained.

Table 3 shows the correctness of classification. Each classified region is manually marked as correct or incorrect. In the data for the year 2002, the total number of classified buildings was 29. All regions were confirmed as true positive regions. Another class was vegetation, with 303 regions. The correctness for regions of vegetation was 92%. The commission regions were buildings with large roughness. In the data for the year 2005, the number of classified buildings had increased to 65 because of urbanization. The correctness of building and vegetation classification was 80% and 90%, respectively. The commission error for buildings was mostly caused by vegetation with low roughness. Overall, the correctness of classification was higher than 80% in our study case.

Four types of change were examined in this study: ‘changed building’, ‘newly built from existing building-to-building’, ‘newly built from non-building-to-building’, and ‘demolished building’. Knowing the accuracy of the assigned change type is critical. The results show that most of the change types are in the ‘newly built from non-building-to-building’ category. They are 42 in number, and the classification accuracy is 74%. The commission error arose primarily from misclassification. Eight newly built buildings changed from old, existing buildings. This number is reasonable, because people seldom demolish a house to build a new one; instead, they renovate or rebuild the old one. Thus, the accuracy achieves 88%. A changed building refers to a building with major structural change. Fifteen regions were defined as changed buildings. Thus, the accuracy is 93%. The number of ‘demolished building’ was 6 with an accuracy of 83%. The total number of changed regions was 71. The number of correct change types was 57. The overall accuracy is 80% in the change-type determination. The results are summarized in Table 4.

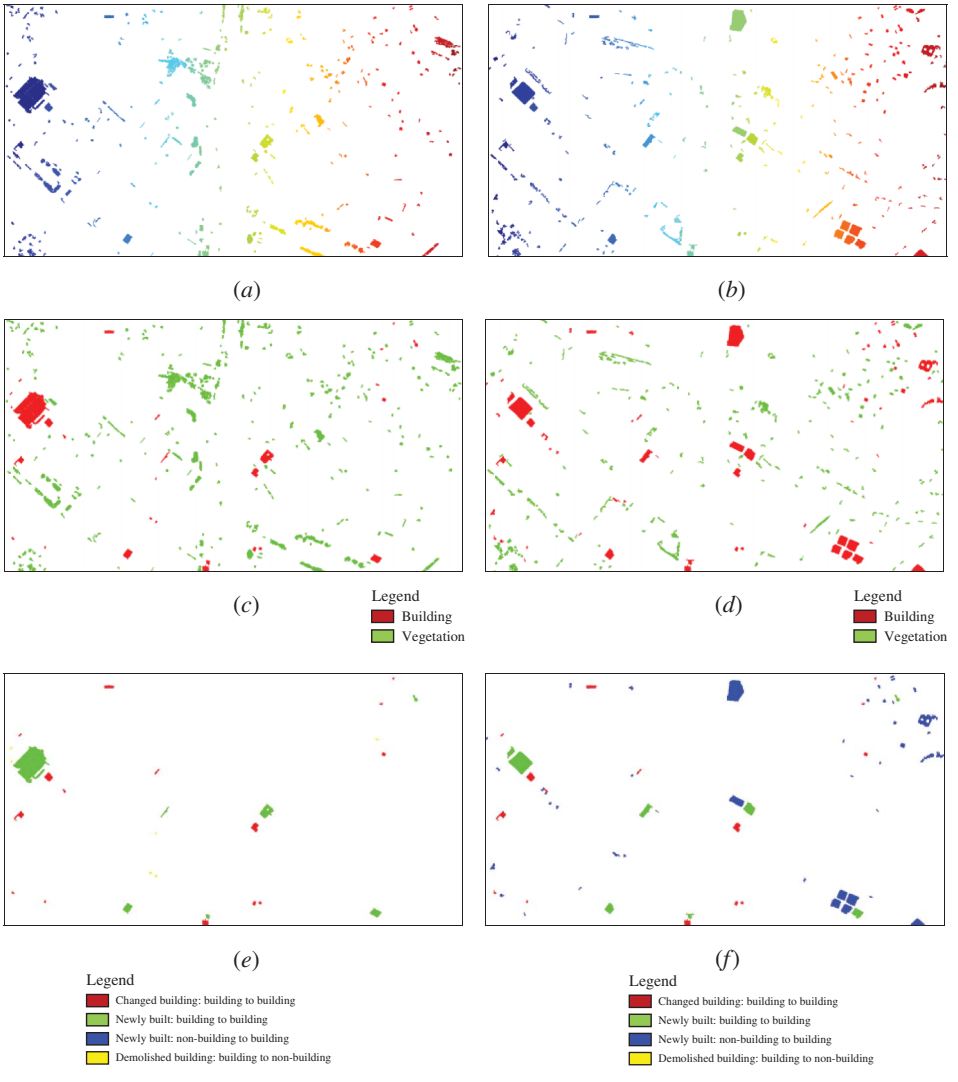

Figure 7. Experimental results: (*a*) segmentation results (colours indicate isolated regions) (2002); (*b*) segmentation results (colours indicate isolated regions) (2005); (*c*) classification results (2002); (*d*) classification results (2005); (*e*) results of changed types (2002); (*f*) results of changed types (2005).

4. Conclusions

This article proposes an object-based change detection scheme to detect changes in buildings using multi-temporal interpolated lidar data. The idea of this approach is to detect the changed objects based on object properties in different periods. This method integrates height differences and above-ground objects to extract the changed objects. The changed objects are classified into buildings and vegetation, based on surface roughness. Finally, the change type is identified with the attributes of the objects. Four change types were examined in this study: changed building, newly built from existing building-to-building, newly built from non-building-to-building, and demolished building.

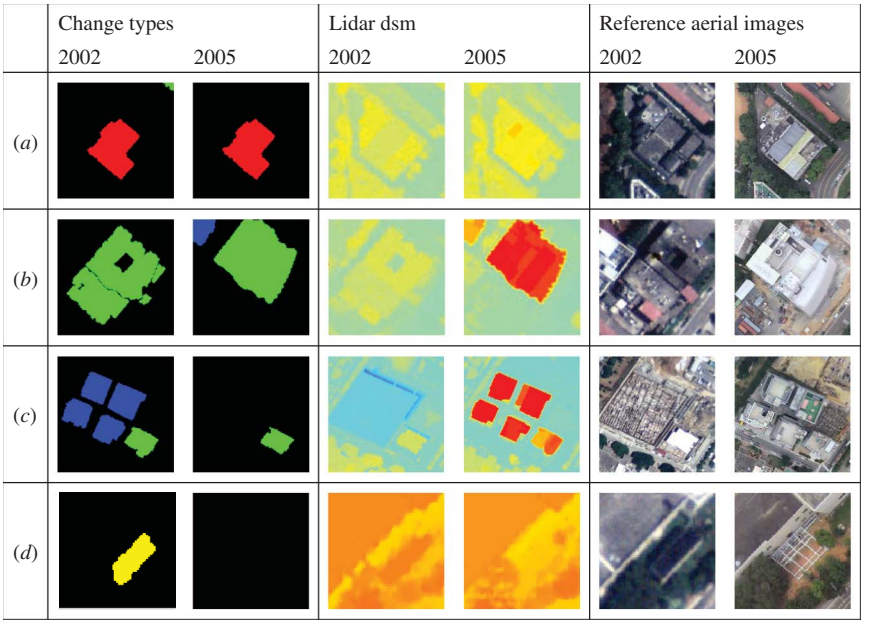

Figure 8. Example of the four categories: (*a*) changed building; (*b*) newly built from existing buildings; (*c*) newly built from non-buildings; (*d*) demolished buildings.

Table 3. Correctness of classification.

	Year 2002		Year 2005	
	Buildings	Vegetation	Buildings	Vegetation
Number of classified regions	29	303	65	246
Number of correct regions	29	279	52	222
Correctness (%)	100	92	80	90

Table 4. Correctness of change-type determination.

	Changed building: building-to-building	Newly built: building-to-building	Newly built: non-building-to-building	Demolished: building-to-non-building
Changed building: building-to-building	14	1	0	1
Newly built: building-to-building	0	7	0	0
Newly built: non-building-to-building	0	0	31	0
Demolished: building-to-non-building	0	0	0	5
Others (vegetation)	1	0	11	0
Total regions/correctness	15/93%	8/88%	42/74%	6/83%

The results indicate that the correctness of classification achieved was 80%. The vegetation with low roughness was the primary cause of the commission error. The results show that 71 regions are marked as changed. From these changed regions, 80% represent real change, while 20% are wrongly classified. The newly built buildings are further classified into 16% of building-to-building, and 84% of non-building-to-building. This can be explained by the fact that the change of non-building-to-building is more cost-effective than that of building-to-building. The proposed method can provide detailed change types to increase the knowledge of change behaviours regarding urban areas.

As most of the errors are caused by the vegetation areas, further study could improve the classification accuracy when additional image data are available. Moreover, improving the accuracy of vegetation classification is possible, as the full-waveform lidar recorded all return echoes. Hence, further techniques could also focus on the change detection using full-waveform lidar.

Acknowledgements

The authors gratefully acknowledge the financial support provided by the CECI Engineering Consultants of Taiwan (Project No. 99922) and the National Science Council of Taiwan (Project No. NSC 100-2221-E-009-133). The authors also thank the Industrial Technology Research Institute of Taiwan for providing the test data and Prof. Bruce King from the Hong Kong Polytechnic University for his assistance.

References

Axelsson, P. 2000. "DEM Generation from Laser Scanner Data Using Adaptive Models." *International Archives of Photogrammetry and Remote Sensing* 33, no. part B4/1: 110–17.

Behan, A. 2000. "On the Matching Accuracy Rasterised Scanning Laser Altimeter Data." *International Archives of Photogrammetry and Remote Sensing* 33, no. part B2: 75–82.

Bouziani, M., K. Goïta, and D.-C. He. 2010. "Automatic Change Detection of Buildings in Urban Environment from Very High Spatial Resolution Images Using Existing Geodatabase and Prior Knowledge." *ISPRS Journal of Photogrammetry and Remote Sensing* 65: 143–53.

Briese, C., N. Pfeifer, and P. Dorninger, 2002. "Application of the Robust Interpolation for DTM Determination." *International Archives of Photogrammetry and Remote Sensing* 33, part B4/1: 55–61.

Caelen, O. 2010. "ARMURS-Automatic Recognition for Map Update by Remote Sensing." *EurSDR Workshop on Automated Change Detection for Updating National Databases*. Accessed February 27, 2011. http://www.eurosdr.net/workshops/cd_2010/p-4.pdf.

Champion, N., L. Matikainen, F. Rottensteiner, X. Liang, and J. Hyyppa. 2008. "A Test of 2D Building Change Detection Methods: Comparison, Evaluation and Perspectives." *International Archives of the Photogrammetry, Remote Sensing and Spatial Information Sciences* 37, part B4: 297–304.

Gruen, A., and D. Akca. 2005. "Least Squares 3D Surface and Curve Matching." *ISPRS Journal of Photogrammetry and Remote Sensing* 59: 151–74.

Hollaus, M., and B. Höfle. 2010. "Terrain Roughness Parameters from Full-Waveform Airborne LiDAR Data." *International Archives of the Photogrammetry, Remote Sensing and Spatial Information Sciences* 38, part 7B: 287–92.

Im, J, J. R. Jensen, and J. A. Tullis. 2008. "Object-Based Change Detection Using Correlation Image Analysis and Image Segmentation." *International Journal of Remote Sensing* 29: 399–423.

Jaw, J. J., and T. Y. Chuang. 2008. "Registration of LiDAR Point Clouds by Means of 3D Line Features." *Journal of the Chinese Institute of Engineers* 31: 1031–45.

Jung, F. 2004. "Detecting Building Changes from Multitemporal Aerial Stereopairs." *ISPRS Journal of Photogrammetry and Remote Sensing* 58: 187–201.

Knudsen, T., and B. P. Olsen. 2003. "Automated Change Detection for Updates of Digital Map Databases." *Photogrammetry Engineering and Remote Sensing* 69: 1289–96.

Li, P., H. Xu, and J. Guo. 2010. "Urban Building Damage Detection from Very High Resolution Imagery Using OCSVM and Spatial Features." *International Journal of Remote Sensing* 31: 3393–409.

Matikainen, L., J. Hyyppä, and H. Hyyppä. 2004. "Automatic Detection of Changes from Laser Scanner and Aerial Image Data for Updating Building Maps." *International Archives of Photogrammetry Remote Sensing and Spatial Information Science* 35: 434–9.

Mass, H.-G. 1999. "The Potential of Height Texture Measures for the Segmentation of Airborne Laser Scanner Data." In *21st Canadian Symposium on Remote Sensing*, Ottawa, June 21–24. Ontario: Canada Remote Sensing Society.

Murakami, H., K. Nakagawa, and H. Hasegawa. 1999. "Change Detection of Buildings Using an Airborne Laser Scanner." *ISPRS Journal of Photogrammetry and Remote Sensing* 54: 148–52.

Rottensteiner, F. 2008. "Automated Updating of Building Data Bases from Digital Surface Models and Multi-Spectral Images: Potential and Limitations." *International Archives of Photogrammetry Remote Sensing and Spatial Information Science* 37, no. B3A: 265–70.

Sithole, G., and G. Vosselman. 2004. "Experimental Comparison of Filter Algorithms for Bare-Earth Extraction from Airborne Laser Scanning Point Clouds." *ISPRS Journal of Photogrammetry and Remote Sensing* 59: 85–101.

Stamm, J. C., and R. Briggs. 1999. "Change Detection in Digital Orthophotos." *Geomatics International Magazine* 13: 44–7.

Steinnocher, K., and F. Kressler. 2006. *Change Detection (Final Report of a EuroSDR Project), EuroSDR Official Publication No. 50*, 111–82, Frankfurt: EuroSDR.

Terrasolid. 2004. *TerraScan User Guide* (18 November 2004). Helsinki: Terrasolid.

Vögtle, T., and E. Steinle. 2004. "Detection and Recognition of Changes in Building Geometry Derived from Multitemporal Laserscanning Data." *International Archives of Photogrammetry Remote Sensing and Spatial Information Science* 35, no. B2: 428–33.

Vosselman, G., B. G. H. Gorte, and G. Sithole. 2004. "Change Detection for Updating Medium Scale Maps Using Laser Altimetry." *International Archives of Photogrammetry Remote Sensing and Spatial Information Science* 35, no. B3: 207–12.

Vu, T. T., M. Matsuoka, and F. Yamazaki. 2004. "LIDAR-Based Change Detection of Buildings in Dense Urban Areas." *IEEE International Geoscience Remote Sensing Symposium* 5: 3413–16.

Vu, T. T., and Y. Ban. 2010. "Context-Based Mapping of Damaged Buildings from High-Resolution Optical Satellite Images." *International Journal of Remote Sensing* 31: 3411–25.

Walter, V. 2004. "Object-Based Classification of Remote Sensing Data for Change Detection." *ISPRS Journal of Photogrammetry and Remote Sensing* 58: 225–38.

Walter, V. 2005. "Object-Based Classification of Integrated Multispectral and LiDAR Data for Change Detection and Quality Control in Urban Areas." *International Archives of Photogrammetry Remote Sensing and Spatial Information Science* 36, no. 8–W27: 1–6.